




Fracture features of anisotropic materials at different impact velocities*

M. N. Krivosheina^a, S. V. Kobenko^b, E. V. Tuch^a , O. A. Kashin^c, A. I. Lotkov^c and Yu. A. Khon^a

^aLaboratory of Physics of Nonlinear Media, Institute of Strength Physics and Materials Science of SB RAS, Tomsk State University, Tomsk, Russia; ^bFaculty of Information Technology and Mathematics, Nizhnevartovsk State University, Nizhnevartovsk, Russia; ^cLaboratory of Shape Memory Alloys, Institute of Strength Physics and Materials Science of SB RAS, Tomsk State University, Tomsk, Russia

ABSTRACT

The paper provides a 3D finite element simulation to investigate the fracture of low-anisotropy aluminium alloy 2024 loaded by a steel impactor at a velocity of 200 and 600 m/s. For aluminium alloy 2024 a failure criterion in terms of ultimate plastic strains is used taking into account the elastic, plastic, and strength anisotropy of the target material. The simulation results, presented as cross-sectional fracture distributions, demonstrate that increasing the impact velocity results in additional fracture zones in anisotropic materials whose elastic, plastic, and strength properties are lowest in the in-plane direction compared to isotropic materials.

ARTICLE HISTORY

Received 24 June 2017
Accepted 15 October 2017

KEYWORDS

3D simulation; finite element method; low-anisotropy aluminium alloy, impact loading, elastic, plastic, and strength anisotropy

Introduction

Moulded metals, as a rule, have low elastic and high strength anisotropy (Vignjevic, Djordjevic, Campbell, & Panov, 2012). The way in which the mechanical anisotropy of a material influences its deformation and fracture depends on the kinematics and geometry of loading and requires complex theoretical and experimental investigations (Beese, Luo, Li, Bai, & Wierzbicki, 2010; Brian, 2005; Rousselier, Barlat, & Yoon, 2009; Steglich, Brocks, Heerens, & Pardoën, 2008; Stoughton & Yoon, 2009; Vignjevic et al., 2012). By now, many papers are available on mathematical modelling of plastically deformed anisotropic materials (Barlat, Lege, & Brem, 1991; Barlat & Lian, 1989; Barlat et al., 1997, 2003), isotropic and kinematic hardening of initially isotropic materials (Cardoso & Yoon, 2009; Geng & Shen, 2002; Olmo & Kachi, 1986; Rousselier et al., 2009; Stoughton & Yoon, 2009), and different fracture mechanisms (Beese et al., 2010; Steglich & Brocks, 1997; Steglich et al., 2008). An efficient approach to research in anisotropic materials is 3D

CONTACT E. V. Tuch  tychka2012@mail.ru

*The work was performed under Fundamental Research Programme of State Academies of Sciences for 2013–2020, projects III.23.1.2, III.23.2.2.

numerical simulation, which allows one to study the influence of each individual characteristic on their deformation (Lee, Lee, & Barlat, 2012; Vignjevic et al., 2012).

The ultimate stresses in anisotropic materials cut out in three mutually perpendicular directions can differ by 10–15%, and their respective ultimate strains can differ 10 times (.03–.3). The first failure criterion for anisotropic materials was proposed by Voigt, late in the nineteenth century, who wrote it as an implicit strain tensor polynomial for crystals. Failure criteria for anisotropic materials can also be expressed in terms of ultimate plugging. Such criteria are often applied to spall fracture of anisotropic metals and alloys (Khan & Liu, 2012; Steglich & Brocks, 1997), but they fail to account for strength anisotropy. Anisotropic polycrystalline materials in some directions are fractured as quasi-brittle and in others as plastic. The fracture of metals and alloys under dynamic loading, particularly under compression, is often described using failure criteria which contain an accumulated plastic strain (Odqvist parameter (ZAMM, 1933)). Knowing the plastic strain accumulated under alternate loading, one can account for microdamage accumulation under dynamic loading (Johnson, 1977; Miklyaev & Fridman, 1986). However, the ultimate plastic strain does not allow us to account for strength anisotropy. Of crucial importance for plastic materials involved in damage accumulation and fracture is the level of accumulated plastic strains. It should also be taken into account that dynamic problems give disproportional histories of deformation with intermediate unloading phases.

Here we propose a failure criterion in which the ultimate plastic strains are expressed through relative residual tensile and shear strains on the axes and in the planes of symmetry, making possible a simulation of microdamage accumulation along each individual symmetry axis of an orthotropic or transtropic material under tension and shear. This failure criterion allows one to detect the most probable zones of local fracture in a material and to account for the history of its microfracturing under deformation. The failure criterion is applied to transtropic aluminium alloy 2024 in a 3D finite element simulation of its dynamic fracture. It is shown that the proposed criterion allows one to simulate ‘plugging’ and crater formation in anisotropic materials and to reveal fracture zones not found in simulations of shock-loaded isotropic materials.

Problem statement

The 3D finite element simulation was performed using original programme packages (Krivosheina, Kobenko, & Kozlova, 2009; Radchenko, Kobenko, & Krivosheina, 2004; Radchenko, Radchenko, Tuch, Krivosheina, & Kobenko, 2012). The numerical finite element method was developed by G.R. Johnson for dynamic loading and is conventionally applied to solve certain problems of contact mechanics (Johnson, 1977). The domain is broken into regular cubic finite elements, each broken into tetrahedrons. Figure 1 shows the initial 3D configuration of an impactor (D_1) and target (D_2). The thickness of the target is 30 mm.

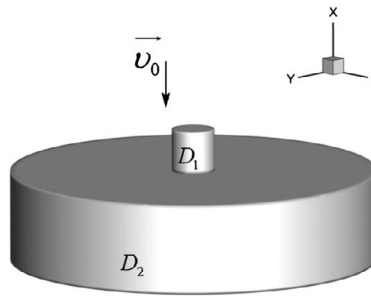


Figure 1. Initial impactor and target configuration.

Elastoplastic deformation of orthotropic material

The system of equations for nonstationary adiabatic motion of a compressible anisotropic medium includes (Sedov, 1976) the continuity equation

$$\frac{\partial \rho}{\partial t} + \text{div} \rho \bar{v} = 0, \quad (1)$$

the equation of motion of a continuous medium

$$\rho \frac{dv^k}{dt} = \frac{\partial \sigma^{ki}}{\partial x_i} + F^k, \quad (2)$$

and the energy equation

$$\frac{dE}{dt} = \frac{1}{\rho} \sigma^{ij} e_{ij}. \quad (3)$$

The symmetric strain tensor is covariant. Here, ρ is the material density; \bar{v} is the velocity vector; F^k are the body force vector components; E is the specific internal energy; σ^{ij} and e_{ij} are the contravariant symmetric stress tensor components and the symmetric strain rate tensor components, respectively. For e_{ij} , we have

$$e_{ij} = \frac{1}{2} (\nabla_i v_j + \nabla_j v_i), \quad (4)$$

where v_i are the velocity vector components; $i, j = 1, 2, 3$.

Let us put that the total strain is the sum of elastic and plastic strains, the plastic flow is independent of hydrostatic pressure (which is possible for materials with low elastic and plastic anisotropy), and the elastic properties of a plastically deformed material are invariant.

The elastic strain in a material is described by generalised Hooke's law:

$$\frac{d\sigma^{ij}}{dt} = C_{ijkl} e_{kl}, \quad (5)$$

with C_{ijkl} being the elastic constant tensor components.

In the plastic range, the total stress tensor is decomposed into spherical and deviatoric components:

$$\sigma^{ki} = -P\delta^{ki} + S^{ki}, \quad (6)$$

where P is the hydrostatic pressure, S^{ki} is the stress deviator components, and δ^{ki} is the Kronecker delta.

The pressure in a material is estimated by the Mie–Grüneisen equation as a function of specific internal energy E and current density:

$$P = \sum_{n=1}^3 K_n \left(\frac{V}{V_0} - 1 \right)^n \left[1 - K_0 \left(\frac{V_0}{V} - 1 \right) / 2 \right] + K_0 \rho E, \quad (7)$$

where K_0, K_1, K_2, K_3 are material constants; V, V_0 are the current and initial volumes.

Let us take the associated flow rule as

$$d\varepsilon_{ij}^p = d\lambda \frac{\partial F}{\partial \sigma^{ij}} \quad (8)$$

where the parameter $d\lambda$, being zero for elastic strain and always positive for plastic strain, is determined from the criterion of yielding; ε_{ij}^p are the plastic strain components; F is the yield function by the von Mises–Hill criterion (Tsai & Wu, 1971).

The von Mises–Hill yield criterion written in terms of stress deviators for an isotropic material with regard to isotropic hardening has the form (Kosarchuk, Kovalchuk, & Lebedev, 1986):

$$F(S^{ij}, R) = \frac{(S^{11})^2}{r_1^2} + \frac{(S^{22})^2}{r_2^2} + \frac{(S^{33})^2}{r_3^2} + \frac{(S^{12})^2}{r_4^2} + \frac{(S^{31})^2}{r_5^2} + \frac{(S^{23})^2}{r_6^2} - R^2 \quad (9)$$

where r_i are determined through tensile and shear yield stresses of a transtropic material, R is the isotropic hardening function. Isotropic hardening assumes a uniform increase in the yield surface during plastic strain accumulation. From experimental research data (Kosarchuk et al., 1986), the function R is invariant to the stress type, is determined from simple loading tests, and is linearly dependent on the accumulated plastic strain θ_{ij}^p :

$$R(\varepsilon_{ij}^p) = 1 + \xi \theta_{ij}^p. \quad (10)$$

The failure criterion for compression and tension of an orthotropic material has the form

$$\theta_{kl}^p \leq \beta_{kl}, \quad k, l = 1, \dots, 3, \quad (11)$$

where β_{kl} is the relative residual strain for compressive and shear fracture of an anisotropic material, and θ_{kl}^p is the plastic strain accumulated by increments of each of its components:

$$\theta_{kl}^p = \int |d \epsilon_{kl}^p|, \quad k, l = 1, \dots, 3.$$

In the failure criterion with ultimate porosity, we can use Herrmann's parameter α which relates the specific volume of a porous material to the specific volume of a solid (initial) material (Herrmann, 1969). The end point of local macroscopic fracture is the instant at which a material reaches its critical porosity: for example, $\alpha = 1.43$ corresponds to 30% porosity and local fracture.

Modifying the failure criterion to model the fracture of anisotropic materials assumes calculations of accumulated plastic strains along each individual symmetry axis and their comparison with ultimate rupture strains in respective directions. Among the variety of fracture types, e.g. plugging, crater formation, spall fracture, brittle failure, radial cracking, petal fracture, etc., the proposed failure criterion as applied to the kinematic and geometric parameters used allows one to model plugging and crater formation with regard to anisotropic material properties.

The stresses in an element rigidly rotated in space are reduced through the Jaumann derivative to the coordinate system

$$\frac{D\sigma^{ij}}{Dt} = \frac{d\sigma^{ij}}{dt} - \sigma^{ik}\omega_{jk} - \sigma^{jk}\omega_{ik}, \quad (12)$$

where $\omega_{ij} = \frac{1}{2}(\nabla_j v_i - \nabla_i v_j)$.

The elastoplastic strain in the impactor was determined in the model for the particular case of an isotropic material. The calculations results for loading of anisotropic material were compared with those for loading of isotropic material with an analysis of mass fraction distributions of fractured elements at the nodes of tetrahedrons. The mass fraction of fractured elements having a common node of the computational domain were determined as

$$R_d = \frac{m_i}{4M},$$

where M is the total node mass, m_i is the total mass fraction of fractured elements. The factor 4 is due to a uniform mass distribution of each tetrahedron between 4 nodes.

The programme uses one system of equations for isotropic and anisotropic materials. The system of equations for isotropic media is a particular case of the deformation theory for anisotropic media. The only ambiguity is in the methods of averaging the mechanical characteristics of an isotropic material from those of an anisotropic material, which is the problem of choice for a researcher.

Numerical simulation results

The model was applied to simulate the fracture of transtropic 2024 aluminium alloy loaded by a compact cylindrical steel impactor of mass 20 g at a velocity of 200 and 600 m/s. The elastic, plastic and strength parameters of the target material for their least values in the impact direction were the following: $\rho = 2700 \text{ kg/m}^3$, $E_x = 86.7 \text{ GPa}$, $E_y = E_z = 92.1 \text{ GPa}$, $\nu_{xy} = .32$, $\nu_{zx} = .34$, $\nu_{yz} = .33$, $G_{xy} = G_{xz} = 33 \text{ GPa}$, $G_{yz} = 31 \text{ GPa}$, $\sigma_{xs} = 290 \text{ MPa}$, $\sigma_{ys} = \sigma_{zs} = 350 \text{ MPa}$, $\tau_{xys} = \tau_{xzs} = 150 \text{ MPa}$, and $\tau_{yzs} = 180 \text{ MPa}$. The ultimate accumulated strains were $\beta_x = .14$, $\beta_y = \beta_z = .2$, $\beta_{xy} = \beta_{xz} = .07$, and $\beta_{yz} = .1$; that is, their ratio in the longitudinal direction was 1:1.43:1.43. Here ρ is density, σ is tensile yield strengths, τ_{ijs} are shear yield strengths, E_i are Young's moduli, G_{ij} are shear moduli, and ν_{ij} are Poisson's ratios for a transtropic material. The isotropic parameters obtained by averaging the transtropic parameters were $E = 87,883 \text{ MPa}$, $G = 32,934 \text{ MPa}$, $\sigma_s = 330 \text{ MPa}$, $\beta = .18$.

The calculation results for loading of transtropic materials with low elongation anisotropy were compared with those of isotropic materials. In the calculations, the mass fractions of compressive and tensile fracture in isotropic material were subtracted from the respective mass fractions in transtropic material. Thus, we determined the differences in the mass fractions of fracture in different target sections. By analysing these differences, we can determine the regions in which fracture initially arises in transtropic and isotropic materials and estimate the time sequence in which individual fracture zones appear in anisotropic materials.

Figure 2 shows the mass fraction difference of fracture in two cross-sections for impact loading transtropic and isotropic materials at 90° , $v_0 = 200 \text{ m/s}$, and $t = 24 \mu\text{s}$. The scale Rd in Figures. 2–5 represents degrees of fracture obtained by subtracting its mass fractions in isotropic material from those in transtropic material. The negative range of Rd indicates that additional fracture zones are present in

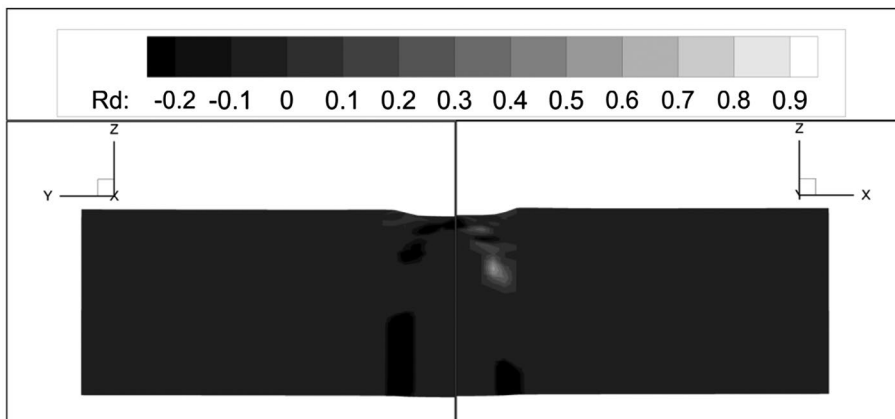


Figure 2. Mass fraction difference for fractured transtropic (1:1.43:1.43) and isotropic materials in compression and tension, Rd , at $v_0 = 200 \text{ m/s}$ and $t = 24 \mu\text{s}$ (degrees of fracture obtained by subtracting its mass fractions in isotropic material from those in transtropic material).

isotropic material and exceed the mass fractions of fracture in transtropic material. The positive range of Rd indicates that the mass fractions of fracture in transtropic material exceed those in isotropic material. The cross-sections in the figures are ZOY (at the left) and ZOX (at the right). The minimum ultimate longitudinal strain is .14 along the axis OX and is .2 along the axes OY and OZ . The differences in the mass fractions of fracture in both sections (in mutually perpendicular directions) are localised beneath the impactor and at the target back surface. Although the impactor by the time point $24 \mu\text{s}$ is bounced off, there is no plugging. In Figure 3, the direction of minimum ultimate strain in transtropic material coincides with the impact direction, and the mass fractions of fracture differ only near the contact zone of the impactor and target. At the target back surface, traces of partial plugging are observed. At $t = 24 \mu\text{s}$, the impactor interacts with the target and its centre-of-mass velocity with respect to the target is 16 m/s. The change in the orientation of minimum elastic, plastic, and strength characteristics of the target material with respect to the impact direction changes the penetration time of the impactor in the target and the degree of its fracture.

Increasing the initial impactor velocity to $v_0 = 600 \text{ m/s}$ increases the fracture volume and the differences in the mass fractions of fractured transtropic and isotropic materials. Figure 4 demonstrates the difference in the mass fractions of fracture in two target cross-sections at $t = 24 \mu\text{s}$. It is seen from the figure that the transtropic material at $v_0 = 600 \text{ m/s}$ reveals additional fracture zones due to shear strains mostly in the ZOX plane in which it is assigned a minimum ultimate strain of .14 along the axis OX (Figure 4, right part). In the target plane ZOY (Figure 4, left part), the isotropic material also reveals additional fracture zones ($Rd < 0$). The target in both cases is fractured through plugging, as can be seen from the geometry of its back surface section.

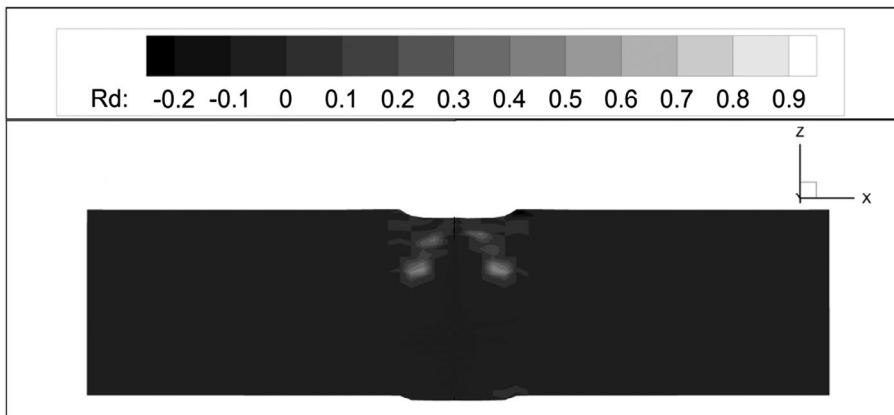


Figure 3. Mass fraction difference for fractured transtropic (1:1.43:1.43) and isotropic materials in compression and tension, Rd , at $v_0 = 200 \text{ m/s}$ and $t = 24 \mu\text{s}$ (degrees of fracture obtained by subtracting its mass fractions in isotropic material from those in transtropic material).

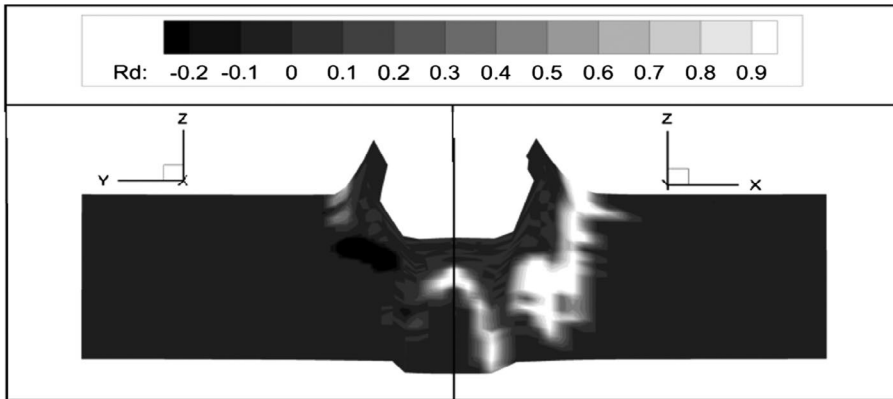


Figure 4. Mass fraction difference for fractured transtropic (1:1.43:1.43) and isotropic materials in compression and tension, Rd , at $v_0 = 600$ m/s and $t = 24 \mu\text{s}$ (degrees of fracture obtained by subtracting its mass fractions in isotropic material from those in transtropic material).

Figure 5 shows the distributions of fracture fields that prevail in transtropic and isotropic target materials under impact load when the orientation of minimum elastic, plastic and ultimate strain (.14) characteristics coincides with the impact direction. The target is also fractured through plugging. The isotropic material reveals additional fracture zones, though its ultimate strain in the impact direction is higher (.18). The volume of additional fracture zones beneath the impactor for the transtropic material is small compared to the isotropic one.

Figure 6–9 show the mass fraction difference individually for compression (Rp) and tension (Rs) at $t = 24 \mu\text{s}$. The negative range of Rp and Rs , like that of Rd , indicates that additional fracture zones are present in isotropic material and exceed the mass fractions of fractured transtropic material. The positive range

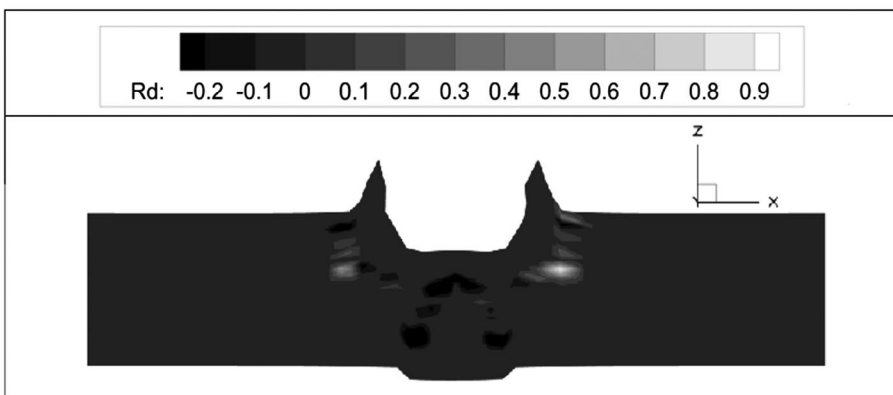


Figure 5. Mass fraction difference of fractured transtropic (1:1.43:1.43) and isotropic materials in compression and tension, Rd , at $v_0 = 600$ m/s and $t = 24 \mu\text{s}$ (degrees of fracture obtained by subtracting its mass fractions in isotropic material from those in transtropic material).

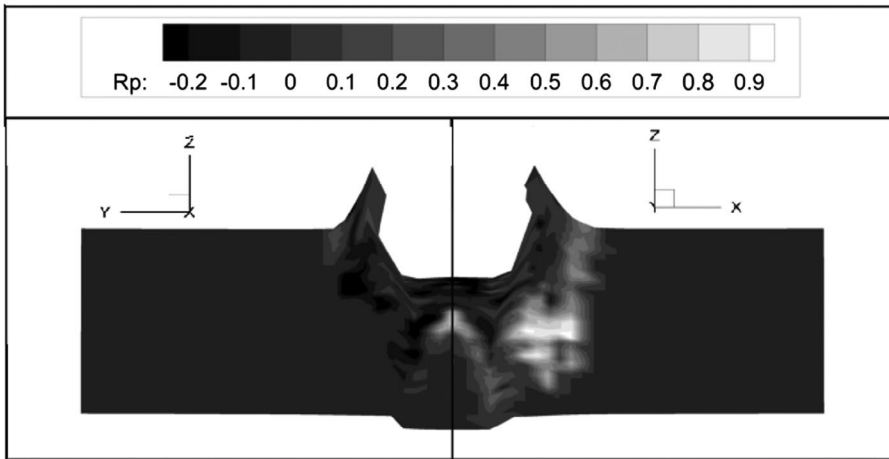


Figure 6. Mass fraction difference for fractured transtropic (1:1.43:1.43) and isotropic materials in compression, R_p , at $v_0 = 600$ m/s and $t = 24$ μ s.

of R_p and R_s indicates that the mass fractions of fracture in transtropic material exceed those in isotropic material.

As can be seen from the data for compression in Figure 7, the additional fracture zones in the isotropic material in Figure 5 are formed in compression waves.

Figure 8 shows how the mass fractions of fracture are distributed in two target cross-sections under tension. Most of the differences in fracture in two materials are found under tension if the minimum elastic, plastic, and strength properties follow the impact direction.

If the direction of minimum ultimate plastic strain (.14) coincides with the impact direction, the differences in fracture in two materials in tension are less pronounced than in compression.

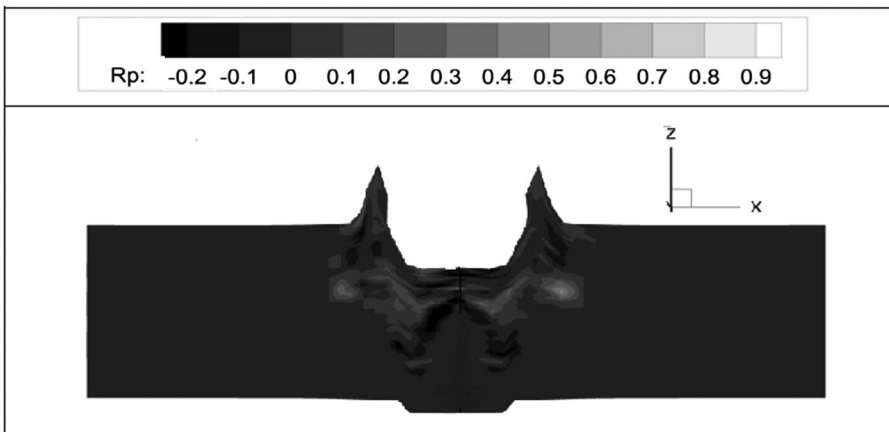


Figure 7. Mass fraction difference for fractured transtropic (1:1.43:1.43) and isotropic materials in compression, R_p , at $v_0 = 600$ m/s and $t = 24$ μ s.

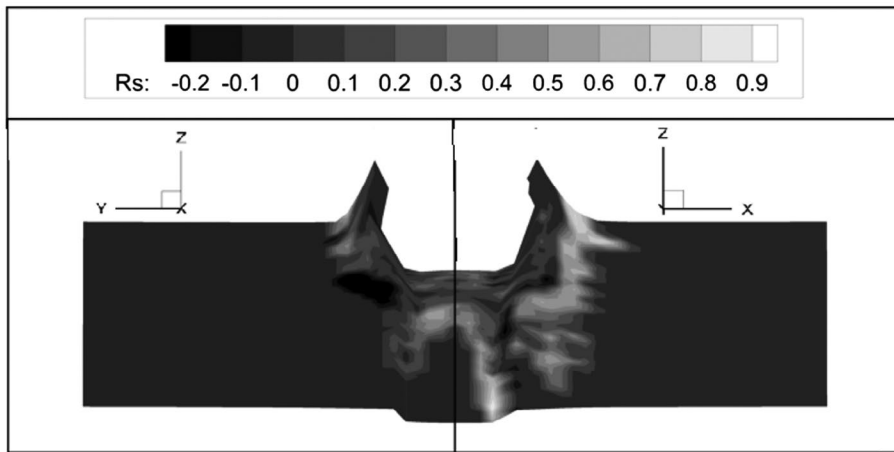


Figure 8. Mass fraction difference for fractured transtropic (1:1.43:1.43) and isotropic materials in tension, R_s , at $v_0 = 600$ m/s and $t = 24$ μ s.

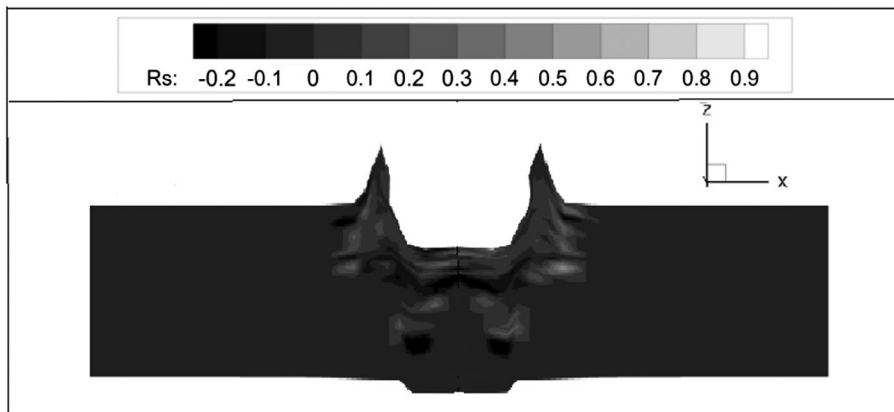


Figure 9. Mass fraction difference for fractured transtropic (1:1.43:1.43) and isotropic materials in tension, R_s , at $v_0 = 600$ m/s and $t = 24$ μ s.

Comparison of the obtained compressive and tensile fracture fields suggests that the largest difference for transtropic and isotropic materials occurs when the minimum ultimate strain (.14) is specified in one of the directions perpendicular to the impact direction; for example, when a rolled material has minimum mechanical properties in a direction perpendicular to rolling. For transtropic materials in which the minimum ultimate strain (.14) acts through the thickness, the mass fractions of fracture differ from those for isotropic materials mostly in compression waves. However, the differences between the mass fractions of fracture in transtropic and isotropic materials under tension and compression are small in this case.

Conclusion

The proposed failure criterion allows one to simulate microdamage accumulation in anisotropic materials and to account for accumulated plastic strain anisotropy in tensile and shear fracture. The application of the criterion to model tensile fracture in isotropic and transtropic materials with low ultimate strain anisotropy shows that at an impact velocity of 200 m/s, irrespective of the orientation of minimum elastic, plastic, and strength properties, the fracture distributions in transtropic materials with low relative residual strain anisotropy (1:1.43:1.43) are close. The simulation of fracture in isotropic materials with average characteristics reveals additional fracture zones which are absent in transtropic materials. Increasing the impact velocity from 200 to 600 m/s adds little to the difference between the fracture patterns in isotropic materials and transtropic materials with minimum elastic, plastic, and strength properties in the impact direction. Increasing the impact velocity slightly increases the zones of fractured transtropic material, particularly if the minimum elastic, plastic, and strength properties are oriented perpendicular to the rolling direction, i.e., parallel to the impact direction. The research data demonstrate that simulations of fracture using the proposed failure criterion, which accounts for microdamage accumulation, make it possible to predict possible fracture scenarios in anisotropic targets and to assess differences in their fracture from fracture in isotropic targets. Among various possible fracture types in targets loaded with initial rates of up to 600 m/s, such as brittle fracture, ductile hole growth, radial fracture, plugging, fragmentation, petaling, crater formation, spalling, etc., this failure criterion allows reliable simulations of only two: plugging and crater formation. Additional studies are needed to determine the range of applicability of the criterion to other fracture types.

Disclosure statement

No potential conflict of interest was reported by the authors.

ORCID

E. V. Tuch  <http://orcid.org/0000-0002-4583-3933>

References

- Barlat, F., Brem, J. C., Yoon, J. W., Chung, K., Dick, R. E., Lege, D. J., ... Chu, E. (2003). Plane stress yield function for aluminum alloy sheets – part 1: Theory. *International Journal of Plasticity*, 19, 1297–1319.
- Barlat, F., Lege, D. J., & Brem, J. C. (1991). A six-component yield function for anisotropic materials. *International Journal of Plasticity*, 7, 693–712.
- Barlat, F., & Lian, K. (1989). Plastic behavior and stretchability of sheet metals. Part I: A yield function for orthotropic sheets under plane stress conditions. *International Journal of Plasticity*, 5, 51–66.

- Barlat, F., Maeda, Y., Chung, K., Yanagawa, M., Brem, J. C., Hayashida, Y., ... Makosey, S. (1997). Yield function development for aluminum alloy sheets. *Journal of the Mechanics and Physics of Solids*, 45, 1727–1763.
- Beese, A. M., Luo, M., Li, Y., Bai, Y., & Wierzbicki, T. (2010). Partially coupled anisotropic fracture model for aluminum sheets. *Engineering Fracture Mechanics*, 77, 1128–1152.
- Brian, N. L. (2005). Effects of geometrical anisotropy on failure in a plastically anisotropic metal. *Engineering Fracture Mechanics*, 72, 2792–2807.
- Cardoso, R. P. R., & Yoon, J. W. (2009). Stress integration method for a nonlinear kinematic/isotropic hardening model and its characterization based on polycrystal plasticity. *International Journal of Plasticity*, 25, 1684–1710.
- Geng, L., & Shen, Y. (2002). Anisotropic hardening equations derived from reverse-bend testing. *International Journal of Plasticity*, 18, 743–767.
- Herrmann, W. (1969). Constitutive equation for the dynamic compaction of ductile porous materials. *Journal of Applied Physics*, 40(6), 2490–2499.
- Johnson, G. R. (1977, March). High velocity impact calculations in three dimension. *Journal of Applied Mechanics*, 95–100
- Johnson, G. R. (1977). High velocity impact calculation in three dimensions. *Journal of Applied Mechanics*, 44 (1), 95–100.
- Khan, A. S., & Liu, H. (2012). Strain rate and temperature dependent fracture criteria for isotropic and anisotropic metals. *International Journal of Plasticity*, 37, 1–15.
- Kosarchuk, V. V., Kovalchuk, B. I., & Lebedev, A. A. (1986). Theory of plastic flow in anisotropic media. Report 1. Determining relationships. *Problem Prochnosti*, 4, 50–56.
- Krivosheina, M. N., Kobenko, S. V., Kozlova, M. A. (2009). Numerical analysis of the effect of isotropic and kinematic hardening of anisotropic targets in impact loading //7th International Conference on Modern Practice in Stress and Vibration Analysis IOP Publishing / Journal of Physics: Conference Series 181 012083 doi:10.1088/1742-6596/181/1/012083 РЕЖИМ доступа: <http://iopscience.iop.org/1742-6596/181/1/012083>
- Lee, J.-W., Lee, M.-G., & Barlat, F. (2012). Finite element modeling using homogeneous anisotropic hardening and application to spring-back prediction. *International Journal of Plasticity*, 29, 13–41.
- Miklyayev, P. G., & Fridman, L. B. (1986). *Anisotropy of mechanical properties of materials*. Moscow: Metallurgia.
- Olmo, N., & Kachi, Y. (1986, June). A constitutive model of cyclic plasticity for nonlinear hardening materials. *Journal of Applied Mechanics*, 53, 395–403.
- Radchenko, A. V., Kobenko, S. V., & Krivosheina, M. N. (2004). Numerical simulation of impact loading of solid propellant within an orthotropic shell. *Space Debris, Kluwer Academic Publishers*, 2(4), 319–330.
- Radchenko, A., Radchenko, P., Tuch, E., Krivosheina, M., & Kobenko, S. (2012). Comparison of application of various strength criteria on modeling of behavior of composite materials at impact. *Journal of Materials Science and Engineering A*, 1, 112–120. (ISSN:2161-6213) (formerly parts of Journal of Materials Science and Engineering ISSN 1934-8959, USA).
- Rousselier, G., Barlat, F., & Yoon, J. W. (2009). A novel approach for anisotropic hardening modeling. Part I: Theory and its application to finite element analysis of deep drawing. *International Journal of Plasticity*, 25, 2383–2409.
- Sedov, L. I. (1976). *Continuum mechanics*. Moscow: Nauka.
- Steglich, D., & Brocks, W. (1997). Micromechanical modeling of the behavior of ductile materials including particles. *Computational Materials Science*, 9, 7–17.
- Steglich, D., Brocks, W., Heerens, J., & Pardoen, T. (2008). Anisotropic ductile fracture of Al 2024 alloys Eng. *Engineering Fracture Mechanics*, 75, 3692–3706.

- Stoughton, T. B., & Yoon, J. W. (2009). Anisotropic hardening and non-associated flow in proportional loading of sheet metals. *International Journal of Plasticity*, 25, 1777–1817.
- Tsai, S. W., & Wu, E. M. (1971). *Journal of Composite Materials*, 5, 58–80.
- Vignjevic, R., Djordjevic, N., Campbell, J., & Panov, V. (2012). Modelling of dynamic damage and failure in aluminum alloys. *International Journal of Impact Engineering*, 49, 61–76.
- ZAMM. (1933). Bd. 13, H. 5, S. 360-363.